

# Preparation for flight testing the VK1 gravity gradiometer

J. Anstie<sup>1</sup>, T. Aravanis<sup>2</sup>, P. Johnston<sup>3</sup>, A. Mann<sup>4</sup>, M. Longman<sup>5</sup>, A. Sergeant<sup>6</sup>, R. Smith<sup>7</sup>, F. Van Kann<sup>8</sup>, G. Walker<sup>9</sup>, G. Wells<sup>10</sup>, and J. Winterflood<sup>11</sup>

<sup>1</sup> University of Western Australia ([anstie@physics.uwa.edu.au](mailto:anstie@physics.uwa.edu.au))

<sup>2</sup> Rio Tinto ([theo.aravanis@riotinto.com](mailto:theo.aravanis@riotinto.com))

<sup>3</sup> University of Western Australia ([pjjohnst@cyclene.uwa.edu.au](mailto:pjjohnst@cyclene.uwa.edu.au))

<sup>4</sup> University of Western Australia ([agm@physics.uwa.edu.au](mailto:agm@physics.uwa.edu.au))

<sup>5</sup> University of Western Australia

<sup>6</sup> University of Western Australia ([anthony.sergeant@uwa.edu.au](mailto:anthony.sergeant@uwa.edu.au))

<sup>7</sup> Greenfields Geophysics ([greengeo@bigpond.net.au](mailto:greengeo@bigpond.net.au))

<sup>8</sup> University of Western Australia ([frank@physics.uwa.edu.au](mailto:frank@physics.uwa.edu.au))

<sup>9</sup> University of Western Australia

<sup>10</sup> Rio Tinto ([geoff.wells@riotinto.com](mailto:geoff.wells@riotinto.com))

<sup>11</sup> University of Western Australia ([jwinter@physics.uwa.edu.au](mailto:jwinter@physics.uwa.edu.au))

---

## Introduction

The VK1 airborne gravity gradiometer is being developed by Rio Tinto in collaboration with the Department of Physics at the University of Western Australia (UWA). The target is to produce an airborne system with a noise level better than 1 Eö in a bandwidth of 1 Hz. Although achieving this performance presents significant challenges for both the instrument and the data processing, it is believed that this level of performance is required for detailed mineral exploration.

This is seen in [Figure 1](#), where the performance of the proposed VK1 instrument is compared with existing airborne gravity tools, using the response of a number of mineral deposits for reference and context. The smallest detectable signal is plotted as a function of the wavelength, which for a compact orebody is approximately twice the spatial extent of the signal. For detailed mineral exploration, wavelengths below about 1 km are of interest since these wavelengths are relevant for detecting the response of compact features at depths of less than 500 m. This region is emphasised in the graph by plotting wavelength on the x-axis with a logarithmic scale. The figure is adapted from a similar graph published on the Fugro web site (FALCON, n.d.; Drinkwater et al., 2006). The signatures for a number of ore bodies are shown. Many are marginally detectable by existing airborne gravity gradiometers, but are easily detectable by an instrument with the target performance of the VK1. Note that none of the mineral deposits shown are detectable by airborne gravimetry except for the Blair Athol coal deposit which has a relatively large footprint measuring 4.3 by 4.0 km and a high  $\sim 1 \text{ g/cm}^3$  density contrast with the host.

The analysis presented in [Figure 1](#) focuses on the detection of discrete orebodies, but with improved signal to noise ratio and better resolution, many more subtle geological features will be mappable. These features will include lithology and perhaps even alteration zones associated with mineralisation. This point is illustrated in [Figure 2 a-c](#), adapted from van Kann (2004) and Dransfield (1994).

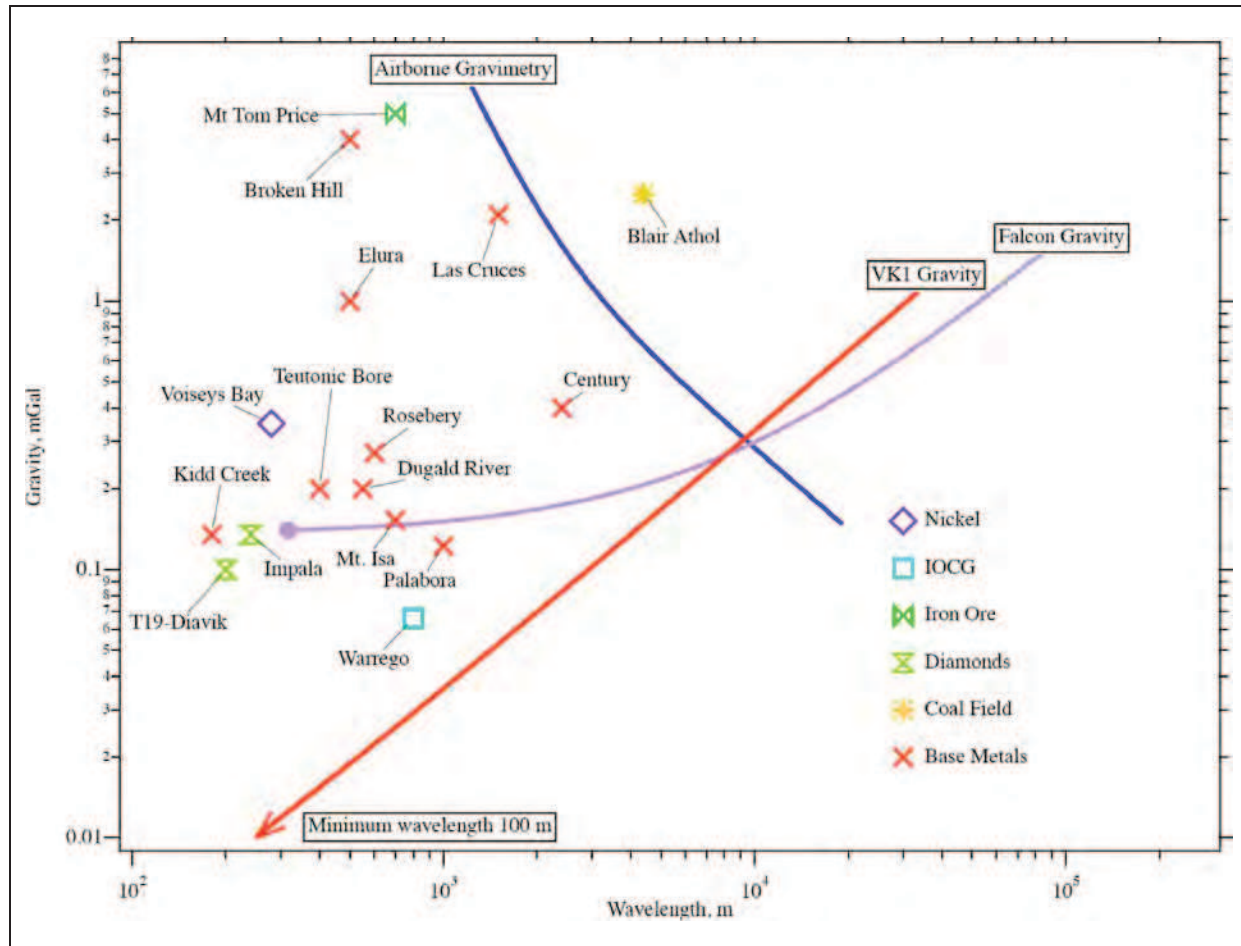


*Figure 1. Detectable gravity signals as a function of wavelength. The three smooth curves represent three types of airborne instrument, as indicated by their respective labels. The curve labelled Airborne Gravimetry represents the limit imposed by the accuracy of the GPS error correction. The curve labelled Falcon Gravity shows the performance of the FALCON system, (FALCON, n.d.), but is also representative of other existing airborne gravity gradiometers. The noise levels of both these and the VK1 gravity gradiometer have been converted to the equivalent gravity errors. These are shown in the context of the response of a selection of compact orebodies, where the wavelength is determined mainly by their depth.*

Unlike instruments currently flying, the sensor in VK1 does not rely on springs or paired accelerometers, but rather the precise balancing of two bars arranged in an "X" fashion, otherwise known as an Orthogonal Quadrupole Responder (OQR). Changes in the gravitational field in the plane of the bars will cause the bars to rotate relative to each other. This rotational movement is directly related to the partial tensor. Although the orientation of the plane of bars can in theory be in any direction, Rio Tinto/UWA have chosen for the sake of simplicity to arrange them vertically, in one of two modes;

- along the nominal flight line direction, measuring a combination of the along line and vertical gravity gradient components, e.g.  $G_{zz} - G_{xx}$  (where  $x$  is the nominal flight direction), or
- at right angles to the nominal line direction, thus a function of the cross-line and vertical gravity gradient, e.g.  $G_{zz} - G_{yy}$ .

The orientation of the instrument is selected by the operator and can easily be changed during a survey, if required.

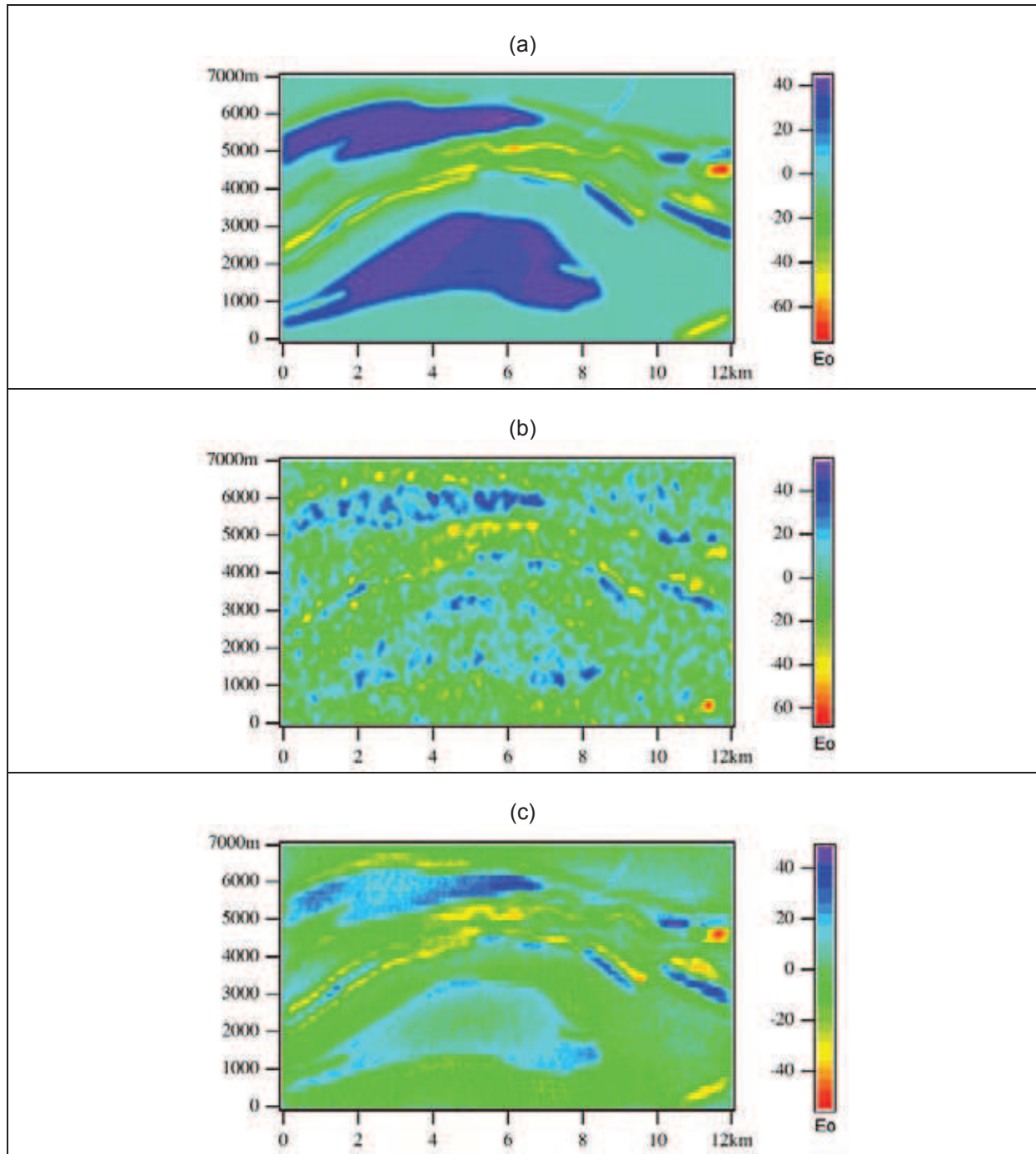


*Figure 2. (a) Noise-free image of simulated Gzz gravity gradient at a terrain clearance of 80 m over Broken Hill prior to mining. The response was calculated at 50 m centres. The response of the orebody and its immediate host is recognisable as a sinuous yellow to orange feature at approximately 5000-9000mE 5000mN. (b) Image of simulated Gzz gravity gradient at a terrain clearance of 80 m and line spacing of 250 m. The modelled instrument measures the component Gxy and the combination  $(G_{xx} - G_{yy})/2$ , and this is used to obtain the component Gzz by standard spatial filtering techniques. The instrumental noise corresponds to 12 Eö/Hz and a filter with a cut-off wavelength of 500 m has been used. (c) Image of simulated Gzz gravity gradient at a terrain clearance of 80 m and line spacing of 250 m. The modelled instrument measures the component Gxy and the combination  $(G_{xx} - G_{yy})/2$ , and this is used to obtain the component Gzz by standard spatial filtering techniques. The instrumental noise corresponds to 1 Eö/Hz and a filter with a cut-off wavelength of 100 m has been used.*

Even in the laboratory, Super conducting Quantum Interference Devices (SQuIDs), operating at liquid helium temperatures, are required to measure the extremely small rotational movement of the bars. In the “hostile” airborne environment, movement of the bars will be influenced by normal translational (i.e. up/down, side to side) and rotational (roll, yaw and pitch) motion of the aircraft. These effects are minimised by precise balancing of the bars and active rotational stabilisation.

Some details of the VK1 instrument were released at the ASEG conference in Adelaide, in February 2009 (Anstie et al., 2009). At that time, the instrument had been partially assembled and had demonstrated a measurement of gravity gradient, in the laboratory, with only partial rotational stabilisation. This paper reports on progress since that date in preparation for flight testing.

## State of preparations for flight testing

The “near flight ready” instrument has measured gravity gradients in the laboratory, both with and without the active stabilisation in operation.

A time record of the gradiometer signal is shown in [Figure 3](#) where a large block of lead is moved towards then away from the instrument (i.e., at approximately 130 and 240 s). These measurements were achieved in a relatively stable environment but with significant micro seismic activity and vibrations produced by researchers working and moving about in the laboratory close to the instrument.

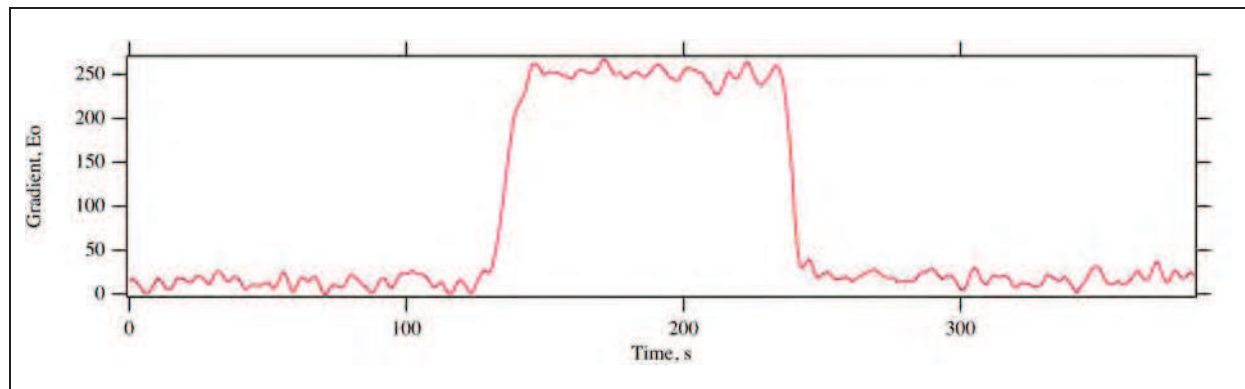


*Figure 3. Time record of the gravity gradient calibration signal (with partial active stabilisation).*

Forward modelling of the effects of the lead block were calculated to give a response of 235 Eö. This provides a useful check of the calibration of the system. The low frequency noise (below about 0.2 Hz) evident in the figure is much larger than the overall system target noise level of 1 Eö in a bandwidth of 1 Hz, and is partly caused by the absence of thermal control, which had not been commissioned at the time.

The dominant cause of the noise is the SQuID itself, whose performance was degraded by environmental factors, predominantly radio frequency interference and cross-talk between the different SQuIDs in the system. This issue has now largely been dealt with.

The full three axis configuration of the instrument has subsequently been assembled for the first time and is undergoing testing in the laboratory. The three axis configuration refers to the number of degrees of freedom in the rotational stabilisation system. The VK1 system has two consecutive stages of rotational stabilisation for each of the three axes of rotation to reach the instruments performance objectives, 1 Eö per root Hz.

The first stage consists of a relatively conventional stabilisation platform between the aircraft and the instrument ([Figure 4](#)). Aircraft rotations are sensed with a state-of the-art Inertial Measurement Unit (IMU) and three gimbal axes controlled by direct-drive torque motors. This platform has already been extensively flight tested and after some minor engineering modifications has produced performances which meet or exceed the design specifications.



*Figure 4. The rotational stabilisation platform, shown mounted in a Cessna 208. The platform (coloured green) stabilises the liquid helium dewar (grey cylinder), which houses the instrument. The instrument is operated in a vacuum inside a sealed chamber, which is immersed in liquid helium.*

The second stage of rotational stabilisation consists of a miniature isolation platform within the instrument itself and operates at cryogenic temperatures. It incorporates frictionless elastic flexures for the gimbal bearings and superconducting actuators for control. Superconducting inertial sensors which measure angular acceleration are used to provide feedback to actively stabilise the instrument. A rotational stabilisation factor of more than 1000 has already been achieved.

In order to prevent the translational acceleration of the aircraft from degrading the rotational control, all three gimbal axes must be extremely well balanced. The requirement is that the centre of mass of the gimbal assembly must be no more than a fraction of a millimetre from the rotation axis. This target has been exceeded by an order of magnitude.

These isolation stages have now been integrated with the instrument and full three axis active control has become operational. It has been extensively tested in the laboratory, both statically and on a recently installed six degrees of freedom flight simulator ([Figure 5](#)). This flight simulator can provide programmed motion with amplitudes approaching 0.5 m and allows most of the aircraft's motion to be reproduced, except for the very low frequency components of the spectrum, below about 0.2 Hz. A second simulator, based on an earth moving machine, can be used to fill-in the low frequency components.

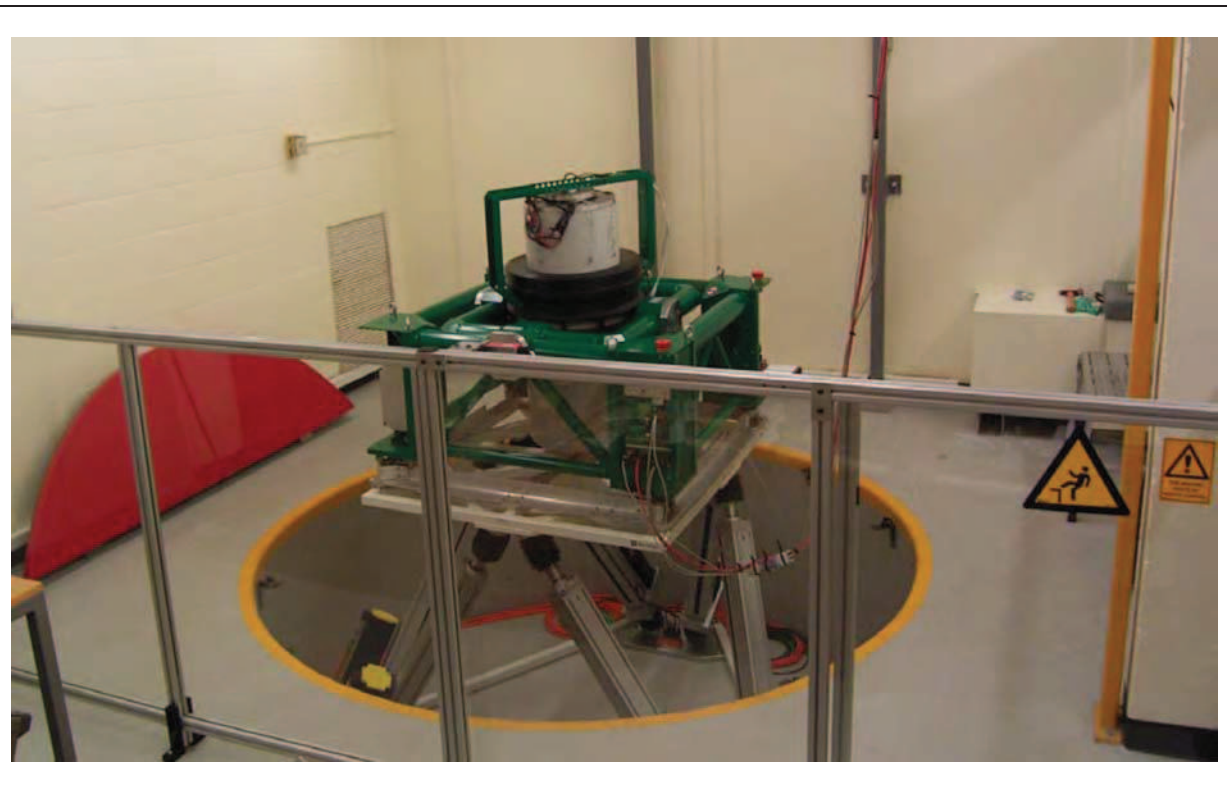


*Figure 5. The instrument being tested on the motion simulator in the laboratory. The simulator can fully reproduce the aircraft motion in the frequency band from 0.4 Hz up to about 50 Hz in all six degrees of freedom.*

The translational acceleration of the aircraft produces forces which are many orders of magnitude greater than the gravity gradient signal. The effects of these forces are minimised by extremely precise balancing of the sensor bars to make their centre of mass coincident with their axis of rotation. A technique has been developed, which positions the centre of mass to within 1 nanometre (about the size of an atom) of the axis of rotation but even this precise balance is insufficient to completely eliminate the effect of the translational acceleration. Three-axis, superconducting linear accelerometers have been developed to measure and compensate for any residual errors produced by translation motion. These accelerometers have been tested separately and have been integrated with the instrument to complete the flight-ready configuration.

The full system is being tested in preparation for flight testing later in 2010. To facilitate these test flights, Rio Tinto has collaborated with the Geologic Survey of Western Australia and Geoscience Australia to establish an AGG test range east of Perth, near the hamlet of Kauaring (Lane et al., 2009). Details of the test range are discussed by Howard et al. (2010) in these workshop proceedings.

In conjunction with instrument development, considerable effort has been expended on preparations for utilising the type of data we expect to acquire. A major contribution to any airborne gravity gradient survey data is likely to be the effects of topography. Since topography may reflect lithology to varying degrees, these effects are not totally unrelated to the geological signals we want to measure, but they do complicate the results and must be addressed. In order to utilise the higher instrument sensitivity, we are striving for better ways to handle topographic effects.

Conventional practise is to apply terrain corrections by calculating the response of the topography using an assumed, usually homogeneous, density contrast at each observation point, and there are many tools available to do this. Spatial algorithms vary in the way they discretise the terrain, in their efficiency and in their ease of use. A number of studies have been conducted both internally and through external groups to assist in optimising these terrain corrections (e.g., Grujic, 2010).

It is essential, of course, to have a sufficiently detailed terrain model to undertake the terrain corrections. In flat area, such as peneplains, freely available SRTM data may suffice. More typically, given the sensitivity of the VK1 system, “bare-earth” LiDAR may be required to either calculate terrain corrections or otherwise incorporate terrain in the interpretation process. Such topographic data are becoming more readily available from a range of sources but, regardless of the accuracy of the terrain model, the terrain correction calculations will always be limited by the appropriateness of the chosen density inputs.

Procedures are available to grid the observed survey data, project them onto a smooth surface or a horizontal plane, and convert the observed quantities into any of the gravity gradient tensor components. Typically these will be  $G_{zz}$  and  $G_z$ . A number of studies have been undertaken to evaluate and improve these processing tools and this work is ongoing. In addition, Rio Tinto is developing tools to predict which targets will be visible to the system after allowing for terrain and terrain clearance effects, expected instrument noise, flight line orientation and host density. These tools will assist users to optimise survey planning and hence maximise the chances of success in various terrains and flying conditions ([Figure 6](#)).

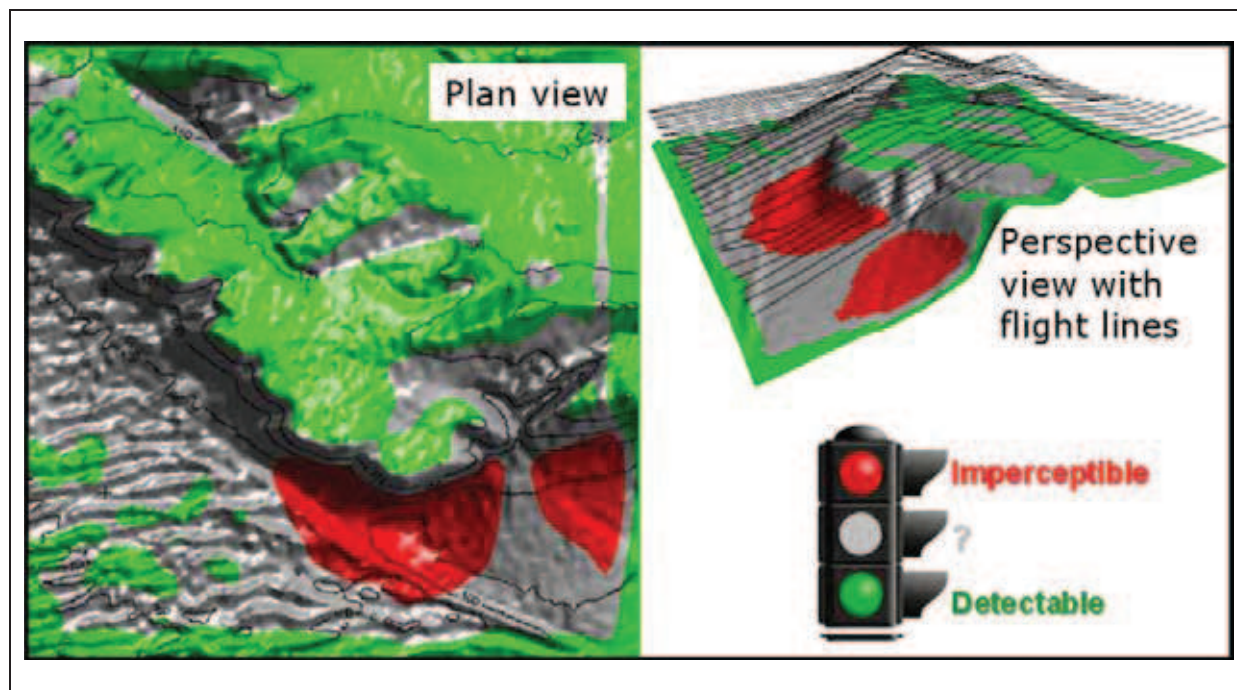


*Figure 6. Example of an AGG simulation, (using Pitney Bowes AGG-SIM software), on shaded and contoured topography. Green signifies where the specific target has sufficient response from background to be detectable. Areas where the target is not detectable are shown in red. Detection is debateable in the grey zones.*

## Acknowledgements

The VK1 system has been developed entirely within the UWA and is wholly funded and owned by Rio Tinto. It will initially be deployed in Australia on Rio Tinto projects but ultimately will be able to operate anywhere in the world.

We would like to thank Rio Tinto for permission to publish the current status of the VK1 project and to thank Richard Lane for his review which greatly improved this paper.

## References

- Anstie, J., Aravanis, T., Haederle, M., Mann, A., McIntosh, S., Smith, R., Van Kann, F., Wells, G., and Winterflood, J., 2009, VK-1 - a new generation airborne gravity gradiometer: Extended Abstract, ASEG-PESA 20th International Geophysical Conference and Exhibition.
- Dransfield, M. H., 1994, Airborne Gravity Gradiometry: Unpub. PhD thesis, University of Western Australia.
- Drinkwater, M. R., Haagmans, R., Muzi, D., Popescu, A., Floberghagen, R., Kern, M., and Fehringer, M., 2006, The GOCE Gravity Mission: ESA's First Core Earth Explorer: 3rd International GOCE User Workshop, Frascati, Italy, 2006, ESA SP-627, 1-8.
- FALCON, n.d., Fugro Gravity & Magnetic Services, Fugro, <http://www.fugro-gravmag.com/FALCON/index.php>, accessed 7 July 2010.
- Grujic, M., 2010, Optimisation of terrain corrections for practical Airborne Gravity gradiometer surveys: Unpub. Bachelor Of Science Honours thesis, Monash University.
- Howard, D., Gujic, M., and Lane, R., 2010, The Kaurong airborne gravity and airborne gravity gradiometer test site, Western Australia: In R. J. L. Lane (editor), Airborne Gravity 2010 Workshop - Abstracts from the ASEG-PESA Airborne Gravity 2010 Workshop: Published jointly by Geoscience Australia and the Geological Survey of New South Wales, Geoscience Australia Record 2010/23 and GSNSW File GS2010/0457.
- Lane, R., Grujic, M., Aravanis, T., Tracey, R., Dransfield, M., Howard, D., and Smith, B., 2009, The Kaurong Airborne Gravity Test Site, Western Australia: Eos Trans. AGU Fall Meeting Supplement, v. 90(52), Abstract G51A-0656.
- Van Kann, F., 2004, Requirements and general principles of airborne gravity gradiometers for mineral exploration: In R.J.L. Lane (editor), Airborne Gravity 2004 - Abstracts from the ASEG-PESA Airborne Gravity 2004 Workshop: Geoscience Australia Record 2004/18, 1-5.